

1 **Ensemble Projection of the Sea Level Rise Impact on Storm Surge
2 and Inundation in the Coastal Bangladesh**

3 Mansur Ali Jisan¹, Shaowu Bao¹, Leonard J. Pietrafesa¹

4 ¹Department of Coastal and Marine Systems Science, Coastal Carolina University, Conway, South Carolina, United States.

5 *Correspondence to:* Mansur Ali Jisan (mjisan@g.coastal.edu)

6 **Abstract.**

7 The hydrodynamic model Delft3D is used to study the impact of Sea Level Rise (SLR) on storm surge and inundation in the coastal
8 region of Bangladesh. To study the present-day inundation scenario, the tracks of two known tropical cyclones (TC) were used:
9 Aila (Category 1; 2009) and Sidr (Category 5; 2007). Model results were validated with the available observations. Future
10 inundation scenarios were generated by using the strength of TC Sidr, TC Aila and an ensemble of historical TC tracks but
11 incorporating the effect of SLR.

12 Since future change in storm surge inundation under SLR impact is a probabilistic incident, that's why a probable range of future
13 change in inundated area was calculated by taking into consideration the uncertainties associated with TC tracks, intensities and
14 landfall timing.

15 The model outputs showed that the inundated area for TC Sidr, which was calculated as 1860 km², would become 31% higher than
16 the present-day scenario if a SLR of 0.26 m occurs during the mid-21st-century climate scenario. Similar to that, an increasing
17 trend was found for the end-21st-century climate scenario. It was found that with a SLR of 0.54 m, the inundated area would
18 become 53% higher than the present-day case.

19 Along with the inundation area, the impact of SLR was examined for the changes in future storm surge level. A significant increase
20 of 14% was found in storm surge level for the case of TC Sidr in Barisal station if a SLR of 0.26 m occurs in the mid-21st-century.
21 Similar to that, an increase of 29% was found in storm surge level with a SLR of 0.54 m in this location for the end-21st-century
22 climate scenario.

23 Ensemble projections based on uncertainties of future TC events also showed that, for a change of 0.54 m in SLR, the inundated
24 area would range between 3500-3750 km² whereas for present-day SLR simulations it was found within the range of 1000-1250
25 km²

26 These results revealed that even if the future TCs remain at the same strength as at present, the projected changes in SLR will
27 generate more severe threats in terms of surge height and the extent of inundated area.

28

29

30

31

32

33 **1. Introduction**

34 In addition to routine inundation from upstream river water and the downstream tides, the coastal part of Bangladesh is frequently
35 flooded by storm surges induced by tropical cyclones (TCs). Typically, TC-induced storm surges in this area initiate in the central
36 or southern part of the Bay of Bengal or near the Andaman Sea. TCs normally occur during April – May, the pre-monsoon period,
37 and again from October – November, the post monsoon period. Harris (1963) mentioned that five basic processes (i.e., pressure,
38 direct wind, earth's rotation, waves and rainfall effects) cause water level rise under storm conditions. Pietrafesa *et al.* (1986) also
39 pointed out that high water at the mouths of coastal estuaries, bays, and rivers can block discharges of upstream waters and
40 contribute to upstream flooding; a non-local effect. Among these processes, storm surges form primarily due to the TC wind
41 stresses mechanically driving the surface frictional layer onshore. Assuming an idealized balance between pressure gradient force
42 and surface wind stress with assumed small bottom stress, the surge related to TC wind stress can be expressed as $\Delta\eta = \frac{\tau_w L}{g\rho h}$, where
43 L is the fetch of the wind (the distance over which the wind blows), τ_w is the wind stress due to the friction between the moving air
44 and water surface, g is the gravity, ρ is the density of water, h is the depth near the coast (Hearn, 2008). Also, as a secondary
45 process, due to the differences in pressure level, the water level rises in the areas of low atmospheric pressure and falls in the areas
46 of high atmospheric pressure, which is how the rising water level offsets the low atmospheric pressure to keep the total pressure
47 constant (Harris, 1963).

48 According to Murty *et al.* (1986), the surge amplifies as it approaches the coast due to the shallow continental shelf of the Bay of
49 Bengal and hence it causes massive flooding in the low-lying coastal areas. A large percentage of the Bangladesh population
50 resides in the low-lying coastal regions of the country. Most of the areas near the coastal zone of Bangladesh have been formed by
51 the process of riverine sedimentation and because of that the low-lying areas are relatively flat and as such are susceptible to
52 flooding even under normal astronomical tide conditions. Furthermore, the triangular shape of the Bay of Bengal region makes
53 storm surges more distressing, as a funneling effect occurs. The geomorphological characteristics of the region have made the
54 locales prone to major TC events, events which have occurred multiple times in the past, directly causing loss of lives, property,
55 livelihoods and the economy of the country (Haque, 1997).

56 Future climate change scenarios may further exacerbate the threats of TC-induced storm surge and inundation. According to the
57 Intergovernmental Panel on Climate Change Fourth Assessment Report (IPCC 4AR), there is a high probability of major changes
58 in TC activity across various ocean basins including the Arabian Sea and the Bay of Bengal. According to Milliman *et al.* (1989),
59 this Ganges-Brahmaputra-Meghna Delta region has long been characterized as a highly vulnerable zone due to its exposure to the
60 increasing trend of SLR. According to the SLR analysis done by the South Asian Association for Regional Cooperation based on
61 the 22-year records of observed sea level at Charchanga, Cox's Bazar and Hiron Point, sea level is rising at rates of 6.0, 7.8 and 4
62 mm/year, respectively in those three locations (SMRC, 2003). These rates are much higher than the global rate of SLR (~ 3.2
63 mm/year) over the last 25 years (Pietrafesa *et al.*, 2015). Based on Warrick *et al.* (1996), the sea level in the Bay of Bengal is also
64 influenced by local factors including tectonic setting, deltaic processes, and sediment load; for example, the coastal region of
65 Bangladesh has been subsiding due to the pressure on the Earth's crust from the sediment with thick layers that have formed over
66 millions of years. Warrick *et al.* (1996) also analyzed the recent history of land accretion and suggested that the subsidence is also
67 balanced by land accretion due to sediment supply from the coast. These physical phenomena have been shaping the coast of
68 Bangladesh over the past 100 years. A global SLR of 26-59 cm has been projected over the next 84 years to 2100 by the IPCC
69 under the scenario A1F1 (Meehl *et al.* 2007). In this proposed work, we will use the SLR projections from Caesar *et al.* (2017;

70 under review), which is based on IPCC AR5 and suggests a projection of SLR of 26 cm for the mid-21st-century (2040 -2060) and
71 54 cm for the end-21st-century (2079 -2099).

72 Previous studies have analyzed the likely impact of climate change, especially SLR, on storm surge and inundation in this region.
73 Using hydrodynamic models, Ali (1992) showed that with an increase of 1.0 and 1.5 m of SLR, 10% and 15.5%, respectively, of
74 the entirety of Bangladesh would get flooded under the strength of future TCs. Karim and Mimura (2008) used a 1-D hydrodynamic
75 model to study the inundation under several scenarios of climate and for the case of future TCs by changing sea surface temperature,
76 SLR, wind speed and sea level pressure. Based on their results, Karim and Mimura (2008) concluded that with an increase of 2°C
77 in SST and 0.3 m of SLR, the flood risk area would be 15.3% more than the present-day risk area and the depth of flooding would
78 increase by as much as 22.7% within 20 km from the coastline. Both Ali (1992) and Karim & Mimura (2008) considered SST rise
79 and future strength of TCs in simulating the future storm surge and inundation.

80 However, the impacts of climate change on the frequency and intensity of TCs are still debatable (Knutson *et al.*, 2010). The
81 projection of the TC characteristics in the Bay of Bengal region is unclear as well. To improve these uncertainties, a reasonable
82 method to examine the impact of future SLR on storm surge and inundation would be to construct an ensemble of tracks and
83 intensities of possible land-falling TCs along the Bangladesh coast based on the historical TC records. From this statistical
84 approach, we can quantify the probable impact of TC tracks under future SLR change. To date, such an approach has not been
85 done and will be the method of this study.

86 We first use Delft3D to simulate the present-day storm surge and inundation using the strength of two recent TCs (Sidr and Aila)
87 and validate the simulations with observational data. Future storm surge and inundation scenarios were then generated by
88 incorporating the projected SLR.

89 The study was carried out in the Ganges-Brahmaputra-Meghna Delta regions (Figure 1a). According to Integrated Coastal Zone
90 Management Plan, 19 districts of Bangladesh located near the Bay of Bengal area were defined as the coastal areas. We've
91 considered all those in this study. We selected two TC cases in this study, a strong Saffir-Simpson(SS) Category-5 that directly hit
92 the study area, TC Sidr, and the other a Category -1 storm that made landfall in the southwest part of the study domain, TC Aila.

93 TC Sidr made landfall near Barguna district (Figure 1a) in 2007, causing ~ 3000 human fatalities and leaving millions homeless.
94 This Category-5 cyclone is considered one of the most powerful cyclones in the past 15 years to have made landfall in Bangladesh,
95 which affected over nine million people living in the Bangladesh coastal areas. The districts of Patuakhali, Khulna, Barguna and
96 Jhalokathi were badly affected. During TC Sidr, around 15% of the affected people took refuge in nearby cyclone shelters. In the
97 village of Angul Kata in Barguna district, around 1500 people took shelter in eight reinforced pillars to protect themselves from
98 the tidal surge of around 5 m. If there had been no shelters, the death toll could have reached into the hundreds in that area.

99 The other cyclone studied in this paper, TC Aila (Figure 1a) occurred in the Bay of Bengal region in 2009. Although a Category-
100 1 storm, Aila caused ~ 190 deaths and affected 4.8 million people, the devastation that left a long-term impact. The locales mainly
101 affected were Khulna, Patuakhali and Chandpur. The storm surge due to Aila broke a dam in Patuakhali and submerged five
102 villages, destroying a huge number of homes and leaving thousands of people homeless. Most of the people living in those affected
103 areas took shelter in the nearest cyclone shelters. According to government sources, approximately 2,500,000 houses had been
104 destroyed completely and 3,700,000 houses had been damaged.

105 The structure of the paper is as follows: brief description of the Delft3D Flow model and the methodologies used to simulate future
 106 changes in storm surge and inundation, to generate ensemble projections of storm surge inundation are discussed in section 2. In
 107 section 3, validation of the model results, present-day storm surge inundation scenarios, ensemble projection of storm surge
 108 inundation and future change in storm surge level ¹are presented. Section 4 includes discussion of model results and the
 109 uncertainties associated with the future projections. Finally, section 5 presents the concluding remarks on research findings.

110 **2. Methodology**

111 **2.1 Modeling Methodology**

112 **2.1.1 Application of Numerical Model**

113 To develop the present-day and future inundation scenario in the coastal regions of Bangladesh, the Delft3D-FLOW (Delft
 114 Hydraulics, 2006), a multidimensional (2D or 3D) hydrodynamic and transport simulation program that calculates non-steady flow
 115 and transport phenomena resulting from tidal and meteorological forcing was used. Delft3D-FLOW solves the unsteady shallow
 116 water equation in two (depth-averaged) or three dimensions. The system of equations consists of the horizontal equations of motion,
 117 the continuity equation, and the transport equations for conservative constituents. The equations are formulated in orthogonal
 118 curvilinear coordinates or in spherical coordinates. Delft3D – FLOW module's two-dimensional, depth averaged flow equations
 119 can be applied for modeling tidal waves, storm surges, tsunamis, harbor oscillations (seiches) and transport of pollutants in
 120 vertically well-mixed flow regimes. In this paper Delft3D's 2D mode for barotropic depth-integrated flow has been applied. The
 121 equations are listed below.

$$122 \frac{\partial \zeta}{\partial t} + \frac{1}{\sqrt{G_{\xi\xi}\sqrt{G_{\eta\eta}}}} \frac{\partial[(d+\zeta)v\sqrt{G_{\eta\eta}}]}{\partial \xi} + \frac{1}{\sqrt{G_{\xi\xi}\sqrt{G_{\eta\eta}}}} \frac{\partial[(d+\zeta)v\sqrt{G_{\xi\xi}}]}{\partial \xi} = Q \quad (1)$$

$$123 \frac{\partial u}{\partial t} + \frac{u}{\sqrt{G_{\xi\xi}}}\frac{\partial u}{\partial \xi} + \frac{v}{\sqrt{G_{\eta\eta}}}\frac{\partial u}{\partial \eta} + \frac{uv}{\sqrt{G_{\xi\xi}\sqrt{G_{\eta\eta}}}}\frac{\partial \sqrt{G_{\xi\xi}}}{\partial \eta} - \frac{v^2}{\sqrt{G_{\xi\xi}\sqrt{G_{\eta\eta}}}}\frac{\partial \sqrt{G_{\eta\eta}}}{\partial \xi} - fv + \frac{g}{\sqrt{G_{\xi\xi}}}\frac{\partial \zeta}{\partial \xi} = -\frac{1}{\rho_0\sqrt{G_{\xi\xi}}}\frac{\partial P_{atm}}{\partial \xi} + F_{\xi} \quad (2)$$

$$124 \frac{\partial v}{\partial t} + \frac{u}{\sqrt{G_{\xi\xi}}}\frac{\partial v}{\partial \xi} + \frac{v}{\sqrt{G_{\eta\eta}}}\frac{\partial v}{\partial \eta} + \frac{uv}{\sqrt{G_{\xi\xi}\sqrt{G_{\eta\eta}}}}\frac{\partial \sqrt{G_{\xi\xi}}}{\partial \eta} - \frac{u^2}{\sqrt{G_{\xi\xi}\sqrt{G_{\eta\eta}}}}\frac{\partial \sqrt{G_{\xi\xi}}}{\partial \eta} + fu + \frac{g}{\sqrt{G_{\xi\xi}}}\frac{\partial \zeta}{\partial \xi} = -\frac{1}{\rho_0\sqrt{G_{\eta\eta}}}\frac{\partial P_{atm}}{\partial \eta} + F_{\eta} \quad (3)$$

125 where ξ , η are the spatial coordinates, ζ is representing water level above some horizontal plane of reference (m), u and v are the
 126 velocities in the ξ and η direction (m/s), d is the water depth below some horizontal plane of reference (m), f is the Coriolis forcing
 127 due to the rotation of the earth, g is the acceleration of gravity (m/s²), P_{atm} is the atmospheric pressure at water surface (kg/m/s²),
 128 Q is the discharge of water, evaporation or precipitation per unit area (m/s) , ρ_0 is the the density of water, $\sqrt{G_{\xi\xi}}$ is the coefficient
 129 used to transfer one coordinate system into another one (m), F_{ξ} is the turbulent momentum flux in ξ -direction (m/s²), F_{η} is the
 130 turbulent momentum flux in η -direction (m/s²). Along with the appropriate set of initial and boundary conditions, the above-
 131 mentioned equations have been solved on an Arakawa-C type finite difference grid. Delft3D- FLOW manual (Delft Hydraulics,
 132 2006) contains detailed information about these numerical aspects.

133 **2.1.2 Model Grid and Bathymetry**

¹ In this paper, the storm surge results refer to the total water level including both normal tides and the water level change due to storm.

134 The grid was set up using spherical coordinates. The grid spacing varies from a minimum of 125 m to a maximum of 1140 m. The
135 finer resolution was applied over land for calculating the inundation or wetting process accurately.

136 In this study, the land topography data were obtained from NASA's Shuttle Radar Topography Mission (SRTM) 90-m resolution
137 datasets (Figure 1b). The bathymetries of the rivers and estuaries are specified using the cross sections measured by the Institute
138 of Water and Flood Management, Bangladesh. The ocean bathymetry was specified using the data from the General Bathymetric
139 Chart of the Oceans 30-arc-sec interval gridded data (BODC, 2003, Figure 1b). Bathymetry and topographic data were interpolated
140 over the model domain using triangular interpolation and grid-cell averaging methods of Delft3D (Delft Hydraulics, 2006).

141 **2.1.3 Wind and Pressure Field**

142 Track data of TCs Sidr and Aila were obtained from the Indian Meteorological Department (www.imd.gov.in). Using those data
143 as input, TC surface winds and mean sea level pressure fields were generated using the Wind Enhancement Scheme (WES)
144 (Heming et al. 1995) method based on the analytical equation by Holland (1980). Delft3D slightly improved the original WES by
145 introducing TC asymmetry. Unlike some previous method that incorporates TC wind asymmetry information from observations
146 (Xie et al. 2006), in WES the asymmetry was brought about by applying the translation speed of the cyclone center displacement
147 as steering current and by introducing rotation of wind speed due to friction (Delft Hydraulics, 2011, Heming et al. 1995).

148 According to the Holland's equation, gradient wind speed $V_g(r)$ at a distance r from the Centre of the cyclone is expressed as the
149 following:

$$150 \quad V_g(r) = \left[\frac{AB(p_n - p_c) \exp\left(-\frac{A}{r^B}\right)}{\rho r^B} + \frac{r^2 f^2}{4} \right]^{0.5} - \frac{rf}{2} \quad (4)$$

151 Here ρ is the density of air, p_c is the central pressure and p_n is the ambient pressure, the Coriolis parameter is represented by f .
152 A and B are determined empirically; with the physical meaning of A as the relation of pressure or wind profile relative to the
153 origin, and parameter B defining the shape of the profile. Delft3D introduces a central pressure drop of $p_d = p_n - p_c$. By equating
154 $\frac{dV_g}{dr} = 0$, and assuming $f=0$ in the region of maximum winds where the Coriolis force is small compared to the pressure gradient
155 and centrifugal forces, the radius of maximum winds R_w can be given as follows:

$$156 \quad R_w = A^{1/B} \quad (5)$$

157 Thus, R_w is independent of the relative values of ambient and central pressure and is defined entirely by the scaling parameters A
158 and B. Substitutions lead to the expression for the maximum wind speed V_m

$$159 \quad V_m = \left[\frac{B p_d}{\rho e} \right]^{0.5} \quad (6)$$

160 Where e is the base of the natural logarithm ($=2.71828182846$).

161 Complete details about this method can be found in the user manual of Delft3D Flow (Delft Hydraulics, 2006), Holland (1980),
162 and Vatvani et al. (2002).

163 The circular grid of TC wind fields used in this study consists of 36 columns and 500 rows and the data were updated at 6 hourly
164 intervals throughout its movement until the landfall. Figure 2 shows a snapshot of the wind field of TC Sidr over the model domain,
165 before landfall, generated using Holland's equation above.

166 **2.1.4 Roughness**

167 The spatially varying Manning's Roughness value was defined based on land cover, such as vegetation, rivers, and ocean (Table
168 1). In the study domain, a mangrove forest, Sundarbans, is located in the Southwest region, near TC Sidr's landfall location (Figure
169 1a). Sakib et al. (2015) found that Sundarban plays a significant role as a buffer in reducing the total inundation during TC passages.
170 Therefore, in this study, the mangrove region was considered. In selecting the roughness values, methods described in Zhang et al.
171 (2012) were followed and slightly modified values were defined for the study area based on the vegetation types in that area.

172 **2.1.5 Boundary conditions**

173 Upstream boundaries were specified as discharges at the mouths of the three major rivers; the Ganges, the Brahmaputra & the
174 Upper Meghna; obtained from the Bangladesh Water Development Board (BWDB) as daily discharge. The downstream ocean
175 boundary was defined by the Topex/Poseidon Inverse Tidal model, based on Egbert et al. (1994). Location of the downstream
176 ocean boundary is shown in Figure 1a.

177 **2.2 Calculation Procedure for Present-day and Future Storm Surge and Inundation Scenario**

178 To generate storm surge and inundation for present-day climate scenario, upstream discharge and downstream water level data
179 from the present-day were used. For future SLR scenarios, present-day hydrodynamic conditions and the strengths of present-day
180 TCs were used but the future sea level was modified based on the SLR projections by Caesar et al. (2017; *under review*). Scenarios
181 were generated for both the mid-21st-century and the end-21st-century time horizons for these TCs, Sidr and Aila. Finally,
182 comparisons were made in terms of storm surge and inundation to identify the changes between present-day and future SLR
183 scenarios.

184 Now, future storm surge inundation due to SLR is a probabilistic event that requires proper addressing of the uncertainties
185 associated with the input parameters. To address the future tropical cyclone uncertainties and obtain statistically significant results,
186 we created an ensemble of tropical cyclone tracks. The ensemble tracks were generated from different historical tropical cyclones
187 that made landfall over the study domain with different intensities (Table 2). Along with the uncertainties associated with future
188 landfall locations, the intensity of Sidr-like and Aila-like TCs may be different. So, to address the uncertainty with the intensity,
189 we increased and decreased their intensity by 10% to simulate a probable range of future storm surge inundation.

190 Storm surge inundation can also be different based on landfall timing. If a storm made landfall during the high astronomical tide
191 condition, its flooding would have been much higher at that time than what could happen during a low astronomical tide condition.
192 For example, the tides shown in Figures 3 and 7 as the water level oscillations have amplitudes as high as 3 m, which could
193 significantly affect the extension of flooded area, depending on whether the storm's landfall coincides with a high tide or a low
194 tide. We note that TC Sidr and TC Aila made landfall during the high tide conditions, which may not always be applicable for the
195 future TCs. To also address uncertainties with the TC landfall timing, experiments were conducted by changing the timing of
196 landfall to identify the impact of high tide and low tide on storm surge and inundation. The change of timing in these tide-related
197 experiments was implemented by modifying the tracks of the storms so that their landfalls coincide with a high tide, a tide, or a

198 zero-tide condition, in addition to their actual tidal phases. Here in this study, future storm surge inundation scenarios caused by
 199 the ensemble tracks will then be simulated by incorporating the projected SLR. By taking all these parameters into consideration,
 200 we conducted a total 108 ensemble simulations (36 for each; present-day and two SLR scenarios). Parameters that were considered
 201 in making ensemble projections are shown in Table 3.

202 **3. Results**

203 **3.1 Validation of the Model**

204 Hourly tidal data from the Bangladesh Inland Water Transport Authority (BIWTA) was used to evaluate the performance of the
 205 model used in this study. The model simulation's root mean square error (RMSE)⁷, mean absolute error (MAE)⁸ and dimension-
 206 less Nash-Sutcliffe coefficient (E)⁹ (Nash and Sutcliffe, 1970) were calculated and listed in Table 4. A Nash-Sutcliffe coefficient
 207 ranges between negative infinity (no skill simulation) and one (perfect simulation).

$$208 \quad RMSE = \sqrt{\frac{\sum_{i=1}^n (X_{obs,i} - X_{model,i})^2}{n}} \quad (7)$$

$$209 \quad MAE = \frac{1}{n} \sum_{i=1}^n |X_{obs,i} - X_{model,i}| \quad (8)$$

$$210 \quad E = 1 - \frac{\sum_{i=1}^n (X_{obs,i} - X_{model})^2}{\sum_{i=1}^n (X_{obs,i} - X_{obs})^2} \quad (9)$$

211 The simulated water levels were compared against the measured data from BIWTA at two locations: Barisal and Charchanga
 212 (Figure 1a). Barisal station is located more towards the inland whereas Charchanga is located near the coastline where the grid cell
 213 resolution was coarse. But none of them are in the open ocean water, which is important to get a clear idea about storm surge level.
 214 TC Sidr made landfall near the Barisal Station (Figure 1a) and the impact of the storm surge was clearer at the Barisal station than
 215 that of TC Aila, which made landfall outside the model domain (Figure 1a); therefore, its impact was not as clear as that of Sidr.
 216 In Figure 3(a) for TC Sidr at the Barisal station, the modeled water level, including storm surge and astronomical tides, was slightly
 217 lower than the observations, and at the Charchanga station (Figure 3b) the measured water level variation displayed smaller
 218 amplitudes than did the model outputs for positive tides, larger amplitudes than the modeled water level for negative tides, perhaps
 219 due to the coarse resolution of bathymetry. Similar types of variations between measured and modeled water level were found for
 220 TC Aila (Figure 3c and Figure 3d). Nevertheless, the modeled water level variations during TCs Sidr and Aila agreed reasonably
 221 well with measured data; as also confirmed by the calculated RMSE, MAE and Nash-Sutcliffe coefficient (Table 4). Therefore,
 222 we conclude that the method can be used to study the impact of SLR on storm surge and inundation in future climate change
 223 scenarios.

224 **3.2 Present-day Inundation Scenario**

225

226 The storm surge inundation scenarios due to the two TCs considered are shown in Figure 4. It can be seen from Figure 4 that the
 227 area flooded by TC Sidr (yellow shade+red shade) was much higher than the area flooded by TC Aila (white shade+red shade),
 228 a result that is consistent with the fact that the category-5 TC Sidr was much stronger than the category-1 TC Aila and directly hit
 229 the study area. The maximum sustained wind speed for TC Sidr was 260 km/h whereas for TC Aila it was 110 km/h. The landfall
 230 location of Sidr was on the Eastern side of Sundarban, while for Aila, the landfall location was towards the Western side of
 231 Sundarbans. That explains why the inundations due to TC Sidr were located near the eastern side of Sundarban, whereas for Aila,

232 the inundation was located mainly in the western part. The extent of inundation due to Sidr (1860 km^2) was 54% larger than that
233 of Aila (1208 km^2)

234 Sakib et al. (2015) showed that Sundarban acted as a buffer zone in reducing the impact of Sidr and thereby reduced much of the
235 potential inundation depth and extent of flooding. As mentioned before, in the model simulation the impact of Sundarban was
236 realized using a higher Manning's roughness value as resistance for the surge to travel.

237 **3.3 Impact of Future Climate Scenarios on Storm Surge Inundation**

238 Future inundation scenarios were generated for two different time horizons: one for the mid-21st-century and the other for the end-
239 21st-century. The initial ocean water level was raised by 0.26 m and 0.54 m for the mid-21st-century and end-21st-century,
240 respectively. The upstream river discharge and downstream ocean water level were used from present-day climate scenarios.

241 In this section we seek to answer the question: if present-day's TCs were to happen in future SLR scenarios, what storm surge and
242 inundation hazard would they cause? Therefore, the tracks and intensities of the two present-day TCs, Sidr and Aila, were used as
243 the model wind input parameters.

244 The model simulated inundated areas and the percent variations were shown in Table 5 and Figure 5. Figure 5 shows that under
245 future SLR scenarios, the inundated areas caused by TCs Sidr and Aila would be significantly higher than those under the present-
246 day climate condition, as indicated by the white color shaded areas. For the category-5 TC Sidr, the inundated area would be 31%
247 (2437 km^2) and 53% (2846 km^2) higher than present-day's 1860 km^2 inundated area, in mid-21st-century (0.26 m SLR) and end-
248 21st-century (0.54 m SLR) climate scenarios, respectively (Figure 5a and Figure 5b)

249 Similarly, for the category-1 TC Aila, there would be an increase in inundated areas. The simulated inundated areas for TC Aila
250 under mid-21st-century and end-21st-century were 1550 km^2 (28%) and 1770 km^2 (47%), respectively (Figure 5c and Figure 5d)
251 whereas for the present-day scenario it was found to be 1208 km^2 .

252 However, in Figure 5, there are several small areas of yellow color indicating zones flooded under present conditions but not
253 flooded during future SLR conditions. This is because Figure 5 showed snapshots of the inundation conditions at one particular
254 time. Some areas may experience alternating wetting and drying conditions, which may explain why some areas are flooded with
255 present SLR and not with higher SLR: this is so only at that particular time. The authors expect that those areas are flooded at other
256 times.

257 All these simulations were carried out using the present-day tides, upstream river discharges and TC tracks and strengths, with
258 only the initial sea water level raised to reflect the effect of the projected future SLR. Therefore, the results suggest that even if the
259 future TCs strengths, tides, and river discharges remain the same as in the present-day climate condition, future SLR would
260 significantly increase the inundated area, by as high as 53%.

261 **3.3.1 Ensemble Projection of Future Storm Surge Inundation under SLR Conditions**

262 As discussed in section 2.2, the future change in storm surge inundation can be different based on the intensity, landfall location
263 and timing of future TCs. By considering all these uncertainty factors mentioned in Table 3, a column plot was created (Figure 6)
264 for present-day sea level and future SLR scenarios. Ensemble simulation outputs also showed an evident increase in the inundated
265 area under the effect of SLR. For the present-day scenario (black column), out of 36 simulations, frequency of storm surge

266 inundation incidents that would likely occur between the range of 1000-1250 km² is 13. whereas for 0.26 m of SLR(red column),
267 peak of the column shifted towards right side with a maximum frequency of inundation events occurred within the range of 2000-
268 2250 km² (10 times out of 36 simulation results). And for 0.54 m of increase in sea level (blue column), the peak of the column
269 shifted more towards the right and the maximum number of simulation outputs (11 out of 36 simulations) showed the range of
270 inundation to be within 3500-3750 km². These results show that even the change in intensities of future TCs are indefinite and the
271 landfall timing is uncertain, increase in sea level is going to increase the area of inundation.

272 **3.4 Impact of Sea Level Rise on Future Storm Surge Level**

273 In addition to the inundation area, SLR would also greatly affect storm surge levels. Similar to the approach used in the inundation
274 study (Section 3.3), TCs Sidr- and Aila-induced storm surges in the future SLR scenarios were simulated using their recorded
275 strengths.

276 The simulated storm surge water levels in future SLR scenarios were compared with both the observed and model generated ones
277 under the present-day scenarios (Figure 7). It is to be mentioned that, while generating the future water level under the effect of
278 SLR, the baseline was only changed by considering the SLR effect and based on that factor the future storm surge level was
279 calculated. Other than that, the water level is the same as present-day TCs.

280 From Figure 7a and Table 6 we can see that for the case of TC Sidr the simulated storm surge level would become 2.13 m in
281 Barisal station which is around 14% higher than the present-day scenario. Similar to that, under the end-21st-century 0.54 m SLR
282 scenario in Barisal, the storm surge would be around 29% higher than the present-day scenario and the peak water level would
283 reach 2.41 m.

284 Increase in storm surge was found at the Charchanga station also. For TC Sidr, under the mid-21st-century scenario (0.26 m SLR),
285 the model simulated storm surge level was found to be 14% higher (1.87 m) than the present-day and 34% higher (2.19 m) (Figure
286 7b, Table 6) than the present-day for the end-21st-century (0.54 m SLR) climate scenario. It is to be noted that, a slight phase shift
287 in the model simulation occurred at this station from November 13 to November 15. This could happen due to the presence of
288 seiche. However, for rest of the period, phase variations are similar to the observed ones.

289 For TC Aila in Barisal, under the mid-21st-century SLR scenario the storm surge would become 22% higher (1.58 m) than the
290 present-day, which was 1.29 m (Figure 7c, Table 6). During the end-21st-century climate scenario, the increment would become
291 even higher as the SLR would be 0.54 m. Storm surge under the 0.54 m end-21st-century SLR condition would be 52% higher
292 (1.96 m) than the present day.

293 At Charchanga, the storm surge would be higher than the present-day condition for TC Aila. Under the 0.26 m mid-21st-century
294 SLR scenario, the storm surge would become 3.07 m which is 23% higher than the present-day condition (Figure 7d, Table 6).
295 And for end-21st-century, this would become 55% higher (3.87 m) than the present day.

296 To analyze the linearity/non-linearity of storm surge level with respect to SLR, we conducted additional experiments based on 5
297 SLR scenarios; present-day sea level, 0.26 m of SLR, 0.33 m of SLR, 0.4 m of SLR, 0.47 m of SLR, 0.54 m of SLR, respectively.
298 Results from these experiments are presented in Table 6.

299 For the case of TC Sidr in Barisal and Charchanga stations, storm surge level increased almost linearly with respect to the addition
300 of water due to the effect of SLR. For example, with a SLR of 0.47 m, the percentage increases in storm surge level with respect

301 to the SLR scenarios in Barisal and Charchanga stations were 96% and 94% m, respectively (Table 6). On the other hand for the
302 case of TC Aila, with a SLR of 0.26 m, the increases in storm surge level were found 112% and 219% respectively for the Barisal
303 and Charchanga station (Table 6). Though the storm surge level is increasing almost linearly with the addition of sea water,
304 however, there are still differences found between them, which could be influenced by the modification of ocean bathymetry to
305 incorporate the effect of SLR. The margin of differences is higher for the case of TC Aila in Charchanga station comparing it with
306 the Barisal station. The coarse resolution of topography near that area might be responsible for that.

307 **4. Discussions**

308 In this paper, we showed that even if the future TCs keep the same strength like the present-day ones their impact will be much
309 higher in a changing climate due to the effect of SLR. Several other factors not included in the modeling could make the storm
310 surge and inundation situation far worse than that shown in the modeling result. These factors include mangrove coverage decrease,
311 morphological changes, TC strength increase, and upstream river discharge changes.

312 For including the effect of future SLR in the model simulations, several methodologies were examined. One of the methods with
313 which we experimented in this study was to include the increased sea level in open ocean boundary instead of adding it in to the
314 whole ocean depth by keeping the coastline fixed. This method was used by some previous studies (Pickering et al. 2012).
315 However, in such a case, an additional pressure gradient force was found acting towards the coast which made the inundated area
316 much higher. Therefore, this method was not used in this study. Instead, in this study, the future SLR was added to the whole ocean
317 domain depth.

318 To make the future SLR simulation realistic, we considered the increased sea level in ocean bathymetry and increased the depth
319 by 0.26 and 0.54 m, respectively, by considering land submergence near the coast. In that case, the result looked much more
320 realistic than the previous one and this is the method we followed in this paper. For example, for the case of TC Aila under the
321 end-21st-century scenario where we used a SLR of 0.54 m SLR at the open ocean boundary instead of adding it to ocean depth and
322 using the hydrodynamic conditions from the present day, the total inundated area was found to be 79% higher than the present-day
323 one. Similar to that, for the mid-21st-century scenario (a 0.26 m SLR), the inundated area was found to be 69% more than the
324 present-day scenario. But when we added the SLR in ocean depth, the mid-21st-century and end-21st-century inundated area were
325 found to be 28% and 47% higher than the present-day scenario. This increase in inundated area was much less than the one that
326 we found by adding the SLR in the open ocean boundary. Figure 8 displays the differences in the inundated area based on the
327 consideration of SLR in the model input.

328 As discussed earlier, TC Sidr made landfall near Sundarban, where the mangrove forest zone acted as a buffer in reducing the
329 impact of the storm surge flood. That is why, even though it was a TC 5, its impact was not as high as it might have been expected
330 to be. In this study, the roughness of the mangrove forest zone on the South-West part of Bangladesh was considered to be fixed
331 for the present-day as well as for future scenarios. But Mukhopadhyay et al. (2015) predicted that 17% of the total mangrove cover
332 could disappear by 2105. If this decreasing trend of vegetation were considered in this study, the flooded area could be much
333 higher.

334 Morphological changes were not considered in this study. But according to Goodbred et al. (2003), each year the eastern, central
335 and western estuaries lose land at a rate of 0.13 cm/year, 0.16 cm/year and 0.16 cm/year, respectively. This could also lead to
336 increased inundated areas for future scenarios. But as the focus of the paper is to estimate the future scenario of storm surge and

338 inundation due to the effect of SLR and to compare with the present-day scenarios, it is important that we keep the roughness and
339 morphological changes constant so that consistent comparisons can be made.

340 Some previous research showed that there could be increases in hurricane strength and landfall probability in the future due to
341 global climate change (Haarsma et al. 2013, Bender et al. 2010, Bengtsson et al. 2007). Though we slightly modified the present-
342 day TC strengths and selected 12 historical TC tracks to reduce landfall uncertainties and to make ensemble projection of future
343 storm surge inundation, strength may be much higher than the ones that we considered for this study. In such case, the devastation
344 could well be much higher under projected SLR conditions, which is very alarming

345 In this paper, we used the present-day river discharge data as an upstream boundary for generating future inundation scenarios.
346 But using the INCA-N, an Inland Catchment Modeling system and considering the projected climatic and socioeconomic scenarios,
347 Whitehead et al. (2015) showed that, there would be a significant increase in future monsoon intensities due to the impact of
348 climate change. That would make future flooding scenarios much worse than those experienced presently. So, based on the changes
349 in TC intensity, river discharges, and land-use changes, the situation could well become more badly impacted than what we found
350 in this study.

351 The findings of our study are important for local governments to consider while they make new management and policy decisions
352 and to improve TC preparedness plans by increasing numbers of shelters and heights. In TC shelters, the first floor should be kept
353 above the high surge waters. Our study showed that, in the future, there would be an increase in surge level from a minimum of
354 14% up to 55% if a TC 1 or a TC 5 makes landfall under increased SLR conditions (Table 6). So, the authority may consider
355 increasing the height of the first floor considering the future risk of an increase in storm surge level and safety of local populations.
356 Also, our model outputs showed that the inundated area increase would range from 28%-53% (Table 5) if there's any TC 1 or TC
357 5 was to make landfall with SLRs of 0.26 m or 0.54 m. This shows that a huge number of new areas are going to face the impacts
358 of storm surge inundation and by considering this issue, it is high time to increase the number of TC shelters in the coastal areas
359 of Bangladesh.

360 **5. Conclusion**

361 Employing the Delft3D-FLOW model, we simulated coastal storm surge and inundation for present-day and future SLR scenarios
362 and compared the changes between them. After validating the present-day model, simulations were conducted for mid-21st-century
363 and end-21st-century climate scenarios where the SLR has been considered as 0.26 m and 0.54 m respectively. The model results
364 showed that, with an increase of 0.26 m and 0.54 m SLR, there would be an increase of 31% and 53% of inundated area respectively
365 if TC Sidr was to made landfall with its present-day strength. There would also be an increase of 28% and 47% in inundated area
366 if Category-1 TC Aila would make landfall with its present-day strength but under SLR of 0.26 m and 0.54 m respectively. Outputs
367 from the ensemble projections showed that, even if the TC intensities, landfall location and timings are uncertain, the most probable
368 range of inundated area extent would shift from 1000-1250 km² (present day) to 2000-2250 km² (under 0.26 m SLR scenario) and
369 3500-3750 km² (under 0.54 m SLR scenario). Besides the inundated area, we also investigated the changes in storm surge level if
370 TC Sidr and TC Aila would make landfall under future SLR conditions. Similar to the inundated area, increases in storm surge
371 levels were found for future scenarios. The significant increase in simulated storm surge and inundation hazards highlights the
372 need for the local governments to improve cyclone preparedness in future SLR scenarios.

374 **Acknowledgement**

375 The authors would like to thank Coastal Carolina University's Cyber-infrastructure project (<http://ci.coastal.edu>) for providing
376 access to computational resources. Also, we would like to acknowledge Dr. Susan Kay from Plymouth Marine Laboratory, UK for
377 her thoughtful opinions regarding the SLR input in model and Institute of Water and Flood Management, Bangladesh for providing
378 important data and support for this work. The authors also appreciate the helpful comments and suggestions from the three
379 anonymous reviewers. The computation was conducted on the Coastal Carolina University Cyber Infrastructure (CI) project and
380 the National Science Foundation's Extreme Science and Engineering Discovery Environment (XSEDE) project.

381 **References:**

382 Ali, A.: Vulnerability of Bangladesh to climate change and sea level rise through tropical cyclones and storm surges, *Climate
383 Change Vulnerability and Adaptation in Asia and the Pacific*, Springer, pp. 171–179., doi: 10.1007/978 94-017-1053-4_16, 1996.

384 Bender, M.A., Knutson, T.R., Tuleya, R.E., Sirutis, J.J., Vecchi, G.A., Garner, S.T., Held, I.M.: Modeled impact of anthropogenic
385 warming on the frequency of intense Atlantic hurricanes, *Science*, 327, 454–458, doi: 10.1126/science.1180568, 2010.

386 Bengtsson, L., Hodges, K.I., Esch, M., Keenlyside, N., Kornblueh, L., LUO, J.-J., Yamagata, T.: How may tropical cyclones
387 change in a warmer climate?, *Tellus a*, 59, 539–561, doi: 10.1111/j.1600-0870.2007.00251.x, 2007.

388 BODC.: Centenary Edition of the GEBCO Digital Atlas, published on CD-ROM on behalf of the Intergovernmental Oceanographic
389 Commission and the International Hydrographic Organization as part of the General Bathymetric Chart of the Oceans. British
390 oceanographic data centre, Liverpool, 2003.

391 Caesar, J., Janes, T., Lindsay, A.: Climate projections over Bangladesh and the upstream Ganges-Brahmaputra-Meghna system,
392 under review, *Environmental Science: Processes & Impacts (Under Review)*, 2017.

393 Delft Hydraulics.: Delft3D-FLOW user manual. Delft, the Netherlands, 2006.

394 Delft Hydraulics.: Wind Enhancement Scheme for cyclone modelling, 2011.

395 Egbert, G. D., Bennett, A. F. and Foreman, M. G. G.: TOPEX/POSEIDON tides estimated using a global inverse model, *J.
396 Geophys. Res.*, 99(C12), 24821–24852, doi:10.1029/94JC01894, 1994.

397 Goodbred, S.L., Kuehl, S.A., Steckler, M.S., Sarker, M.H.: Controls on facies distribution and stratigraphic preservation in the
398 Ganges–Brahmaputra delta sequence, *Sedimentary Geology*, 155, 301–316, doi:10.1016/S0037-0738(02)00184-7, 2003.

399 Haarsma, R.J., Hazeleger, W., Severijns, C., Vries, H., Sterl, A., Bintanja, R., Oldenborgh, G.J., Brink, H.W.: More hurricanes to
400 hit western Europe due to global warming, *Geophysical Research Letters*, 40, 1783–1788, doi: 10.1002/grl.50360, 2013.

401 Haque, C.E.: Atmospheric hazards preparedness in Bangladesh: a study of warning, adjustments and recovery from the April 1991
402 cyclone, *Earthquake and Atmospheric Hazards*, Springer, pp. 181–202, doi: 10.1007/978-94-011-5034-7_6, 1997.

403 Harris, D. L.: Characteristics of the hurricane storm surge, *Tech. Pap.*, 48, U. S. Weather Bur., Washington, D. C., 139 pp, 1963.

404 Hearn, C. J.: The dynamics of coastal models. Cambridge University Press, 2008.

405 Heming, J. T., Chan, J. C. L. and Radford, A. M.: A new scheme for the initialization of tropical cyclones in the UK Meteorological
406 Office global model, *Met. Apps*, 2, 171–184, doi:10.1002/met.5060020211, 1995.

407 Holland, G. J.: An analytic model of the wind and pressure profiles in hurricanes, *Monthly weather review*, 108(8), 1212-1218,
408 doi:10.1175/1520-0493(1980)108<1212:AAMOTW>2.0.CO;2, 1980.

409 Karim, M.F., Mimura, N.: Impacts of climate change and sea-level rise on cyclonic storm surge floods in Bangladesh, *Global
410 Environmental Change*, 18, 490–500, doi: 10.1016/j.gloenvcha.2008.05.002, 2008.

411 Knutson, T.R., McBride, J.L., Chan, J., Emanuel, K., Holland, G., Landsea, C., Held, I., Kossin, J.P., Srivastava, A.K., Sugi, M.:
412 Tropical cyclones and climate change, *Nature Geoscience*, 3, 157–163, doi: 10.1038/ngeo779, 2010.

413 Meehl, G.A., Covey, C., Delworth, T., Latif, M., McAvaney, B., Mitchell, J.F.B., Stouffer, R.J., Taylor, K.E., and. Coauthors,:
414 Global climate projections. *Climate Change 2007: The Physical Science Basis*, S. Solomon et al., Eds. Cambridge University Press,
415 2007.

416 Milliman, John D., James M. Broadus, and Frank Gable.: Environmental and economic implications of rising sea level and
417 subsiding deltas: the Nile and Bengal examples, *Ambio*, 18 (6), 340-345, doi: , 1989.

418 Mukhopadhyay, A., Mondal, P., Barik, J., Chowdhury, S.M., Ghosh, T., Hazra, S.: Changes in mangrove species assemblages and
419 future prediction of the Bangladesh Sundarbans using Markov chain model and cellular automata, *Environmental Science:*
420 *Processes & Impacts*, 17, 1111–1117, doi: 10.1039/C4EM00611A, 2015

421 Murty, T.S., Flather, R.A., Henry, R.F.: The storm surge problem in the Bay of Bengal. *Progress in Oceanography*, 16, 195–233,
422 doi: 10.1016/0079-6611(86)90039-X ,1986.

423 Nash, J.E., Sutcliffe, J.V.:River flow forecasting through conceptual models part I—A discussion of principles, *Journal of*
424 *hydrology*, 10, 282–290, doi:10.1016/0022-1694(70)90255-6, 1970.

425 Pietrafesa, L. J., Janowitz, G. S., Chao, T. Y., Weisberg, R. H., Askari, F., & Noble, E.: The physical oceanography of Pamlico
426 Sound. University of North Carolina Sea Grant Publication UNC-WP-86-5, Raleigh, North Carolina, 125, 1986

427 Pietrafesa, L.J., Bao, S., Yan, T., Slattery, M., Gayes, P.T.: On Sea Level Variability and Trends in United States Coastal Waters
428 and Relationships with Climate Factors, *Advances in Adaptive Data Analysis*, 7, 1550005, doi: 10.1142/S1793536915500053,
429 2015.

430 Pickering, M. D., Wells, N.C., Horsburgh, K. J., and Green, J. A. M.: The impact of future sea-level rise on the European Shelf
431 tides. *Continental Shelf Research* 35: 1-15, doi:10.1016/j.csr.2011.11.011, 2012.

432 Sakib, M., Nihal, F., Haque, A., Rahman, M., Ali, M.: Sundarban as a Buffer against Storm Surge Flooding, *World Journal of*
433 *Engineering and Technology*, 3, 59, doi: 10.4236/wjet.2015.33C009, 2015.

434 SMRC.: The Vulnerability Assessment of the SAARC Coastal Region due to Sea Level Rise: Bangladesh Case, SAARC
435 Meteorological Research Center, Dhaka SMRC-No. 3, 2003.

436 Vatvani, D.K., Gerritsen, H., Stelling, G. S., Rao, A. K.: Cyclone induced storm surge and flood forecasting system for India.
437 *Solutions to Coastal Disasters '02*, San Diego, CA, 2002.

438 Warrick, R.A., Bhuiya, A.A.H., Mitchell, W.M., Murty, T.S., Rasheed, K.B.S.: Sea-level Changes in the Bay of Bengal, in: *The*
439 *Implications of Climate and Sea–Level Change for Bangladesh*, Springer, pp. 97–142, 1996.

440 Whitehead, P.G., Barbour, E., Futter, M.N., Sarkar, S., Rodda, H., Caesar, J., Butterfield, D., Jin, L., Sinha, R., Nicholls, R., others.:
441 Impacts of climate change and socio-economic scenarios on flow and water quality of the Ganges, Brahmaputra and Meghna
442 (GBM) river systems: low flow and flood statistics, *Environmental Science: Processes & Impacts*, 17, 1057–1069, doi:
443 10.1039/C4EM00619D, 2015.

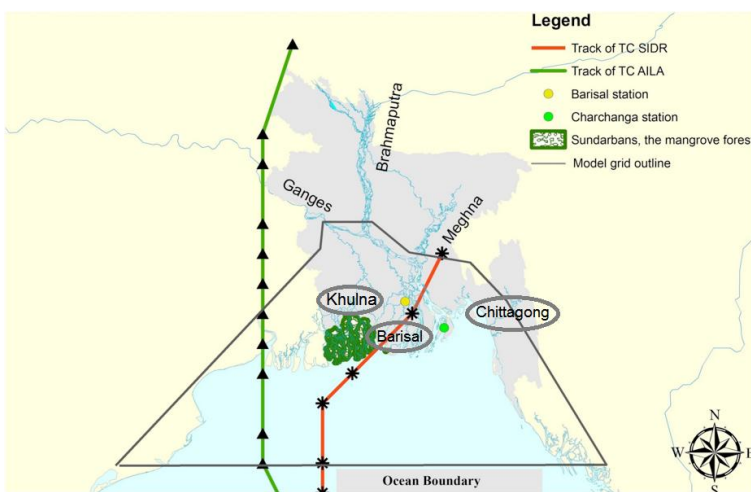
444 Xie, L., Bao, S., Pietrafesa, L.J., Foley, K., Fuentes, M.: A real-time hurricane surface wind forecasting model: Formulation and
445 verification, *Monthly Weather Review*, 134, 1355–1370, doi:10.1175/MWR3126.1, 2006.

446 Zhang, K., Liu, H., Li, Y., Xu, H., Shen, J., Rhome, J., Smith, T.J.: The role of mangroves in attenuating storm surges, *Estuarine,*
447 *Coastal and Shelf Science* 102, 11–23, doi: 10.1016/j.ecss.2012.02.021, 2012.

448

449
450
451
452
453
454
455
456
457
458

(a) Study Area



(b) Topography and Bathymetry

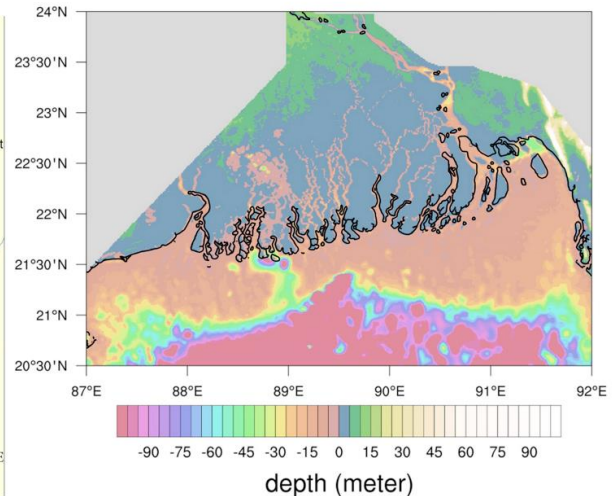


Figure 1. (a) Map of the study area for this work. The red and green lines represent the tracks of TC Sidr and TC Aila respectively. The area marked with green color indicates the Sundarban mangrove forest region. Location of the Ganges, Brahmaputra and Meghna rivers are shown on the map. Khulna, Barisal and Chittagong which are landfall locations for the historical TCs used for ensemble projection, are shown inside a circular box on the map. Two circles over the study area are the observation stations of Bangladesh Inland Water Transport Authority (BIWTA). The black colored outline shows the extent of model grid over the region. (b) Topography and bathymetry of the model domain. Negative depth values represent water bodies (ocean and rivers) and positive depth values areas represent land.

459

460

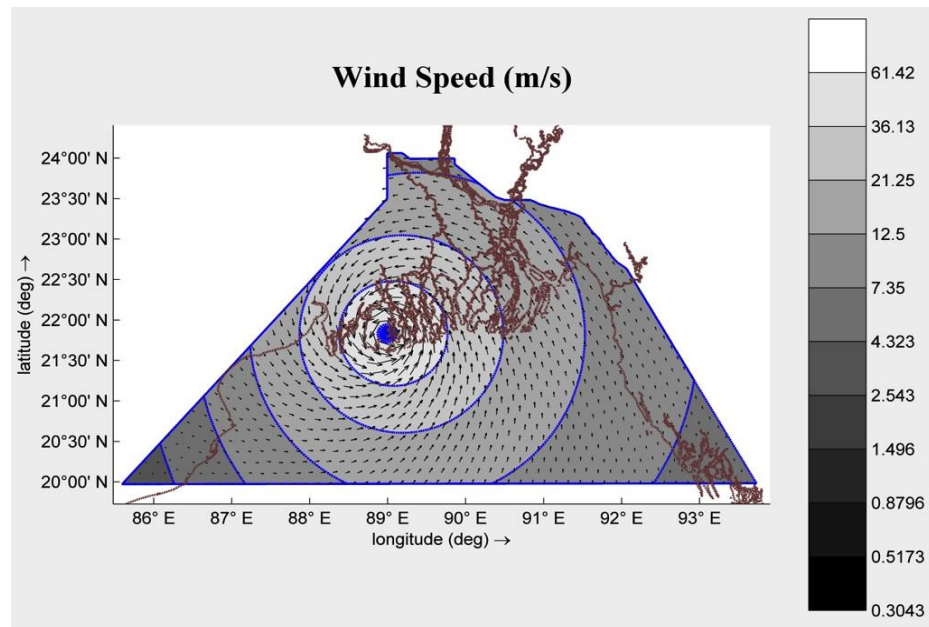


Figure 2. Distribution of the wind field over the model domain for TC Sidr during landfall generated using Holland's Equation.

461

462

463

464

465

466

467

468

469

470

471

472

473

474

475

476

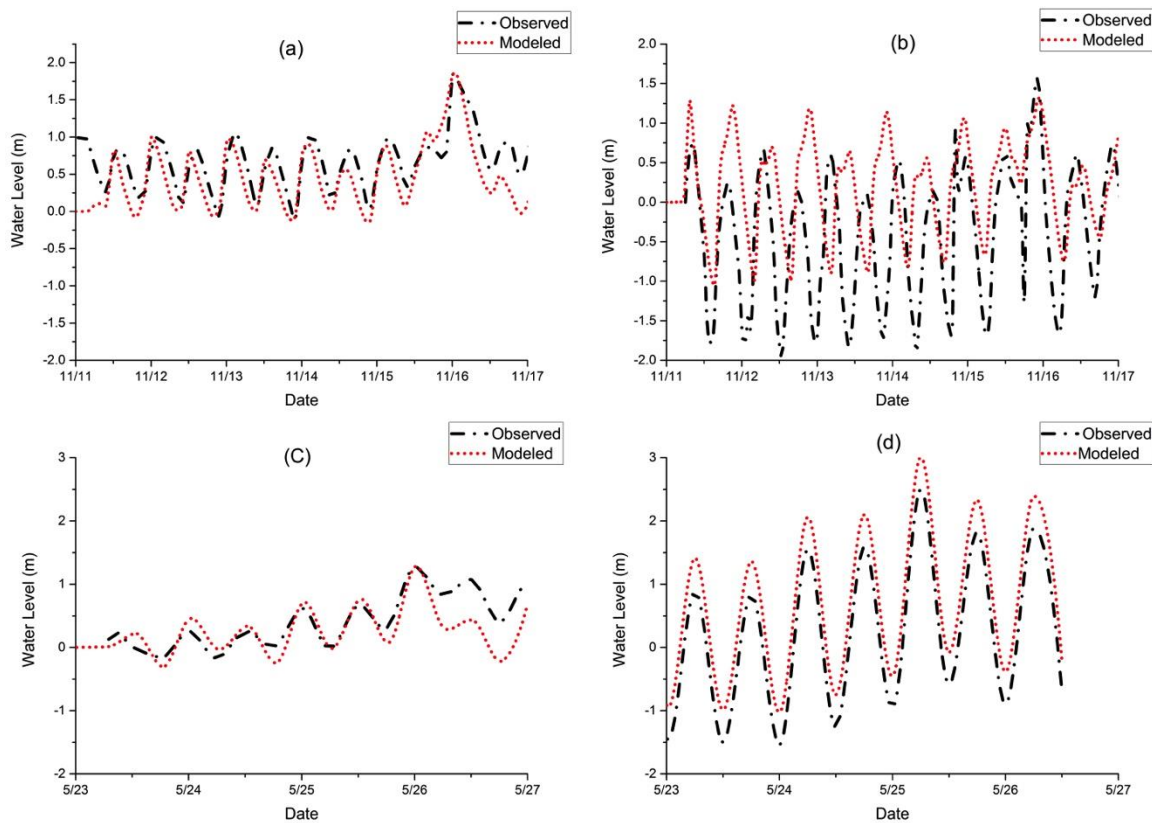


Figure 3. Comparison of observed and modeled water level for TC Sidr and TC Aila in Barisal and Charchanga observation stations. (a) measured and modeled water level comparison for TC Sidr in Barisal (b) TC Sidr in Charchanga (c) TC Aila in Barisal (d) TC Aila in Charchanga.

Comparison of Inundated Area between TC Sidr and TC Aila under Present Day Scenario

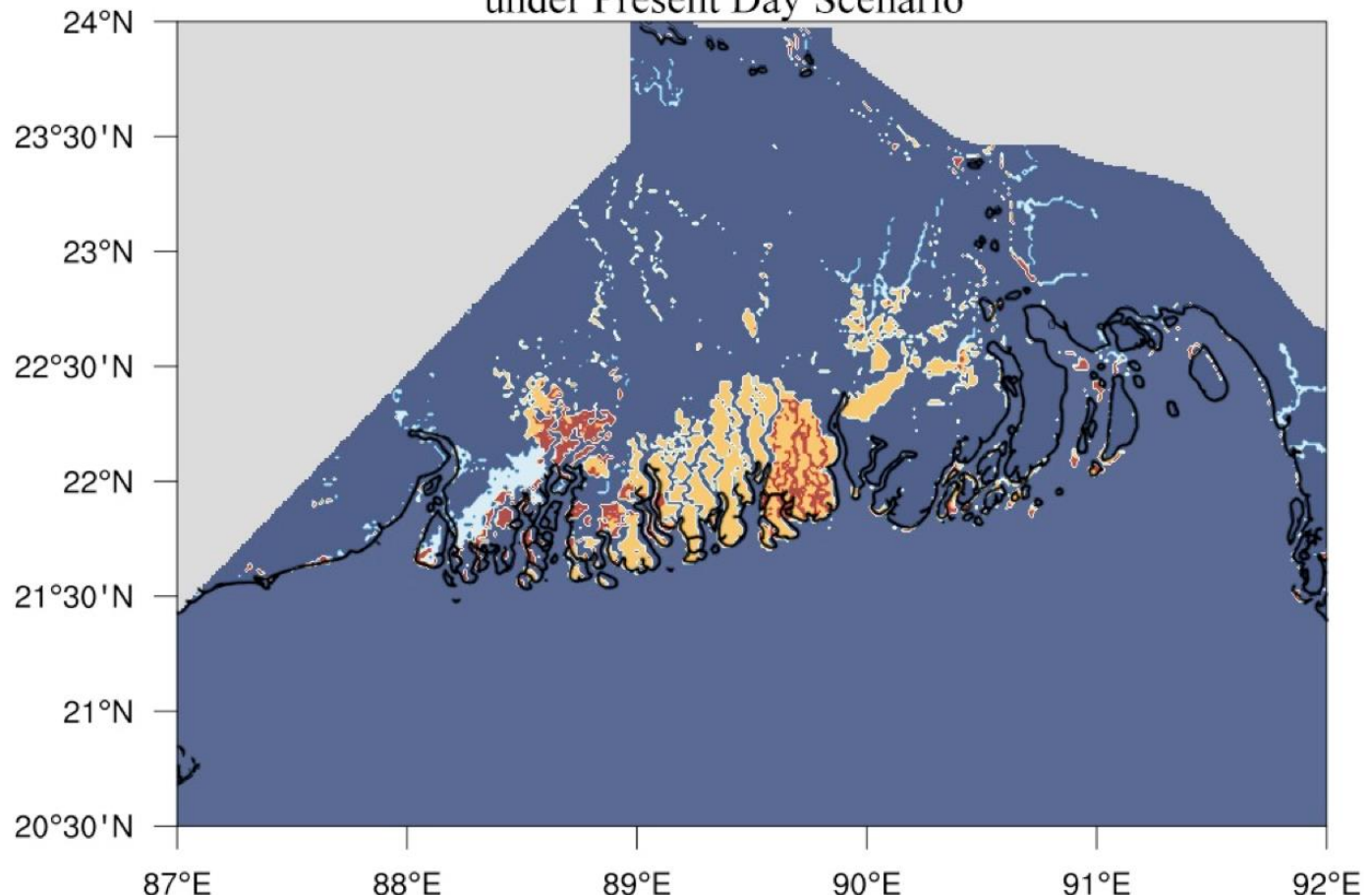
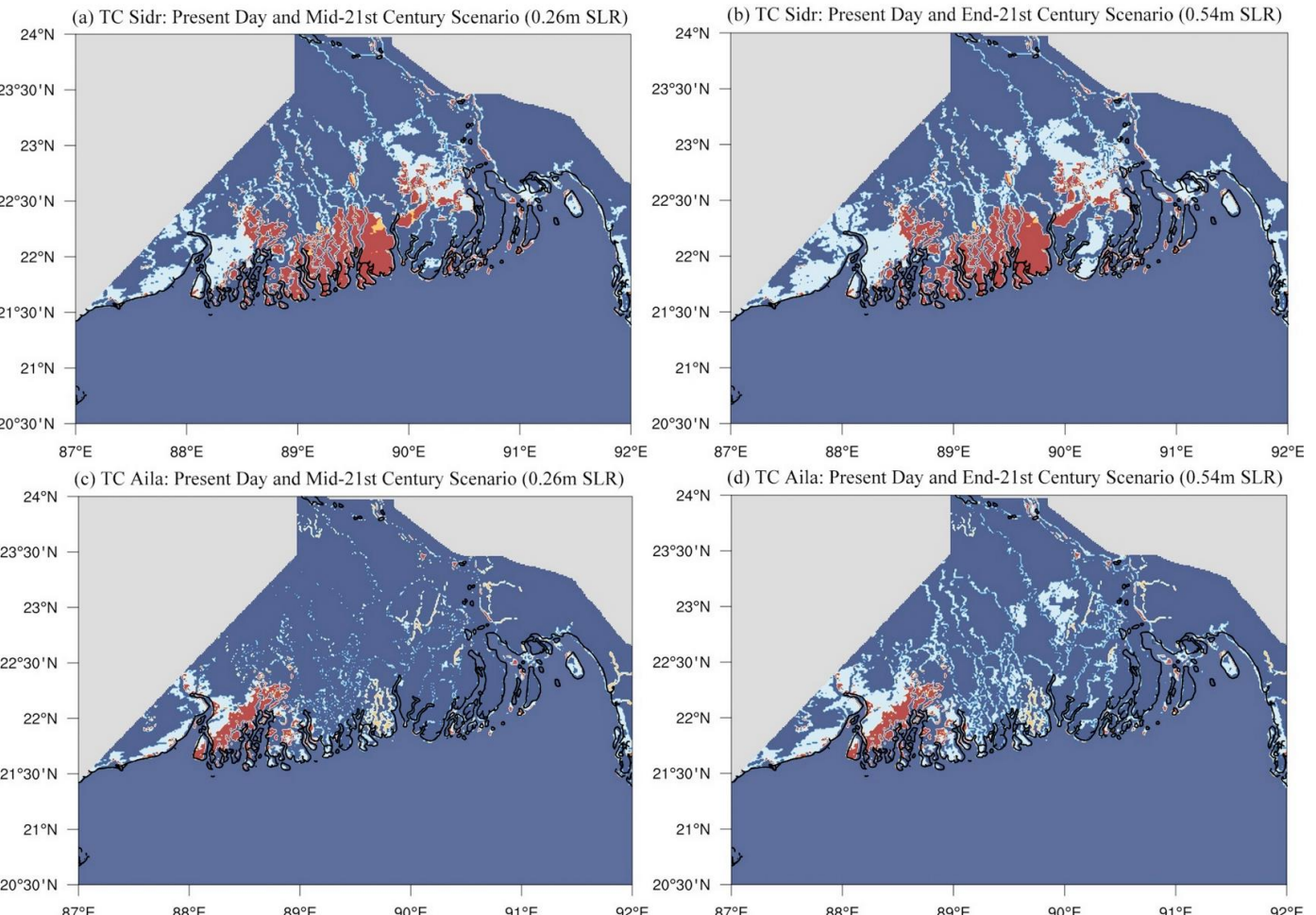
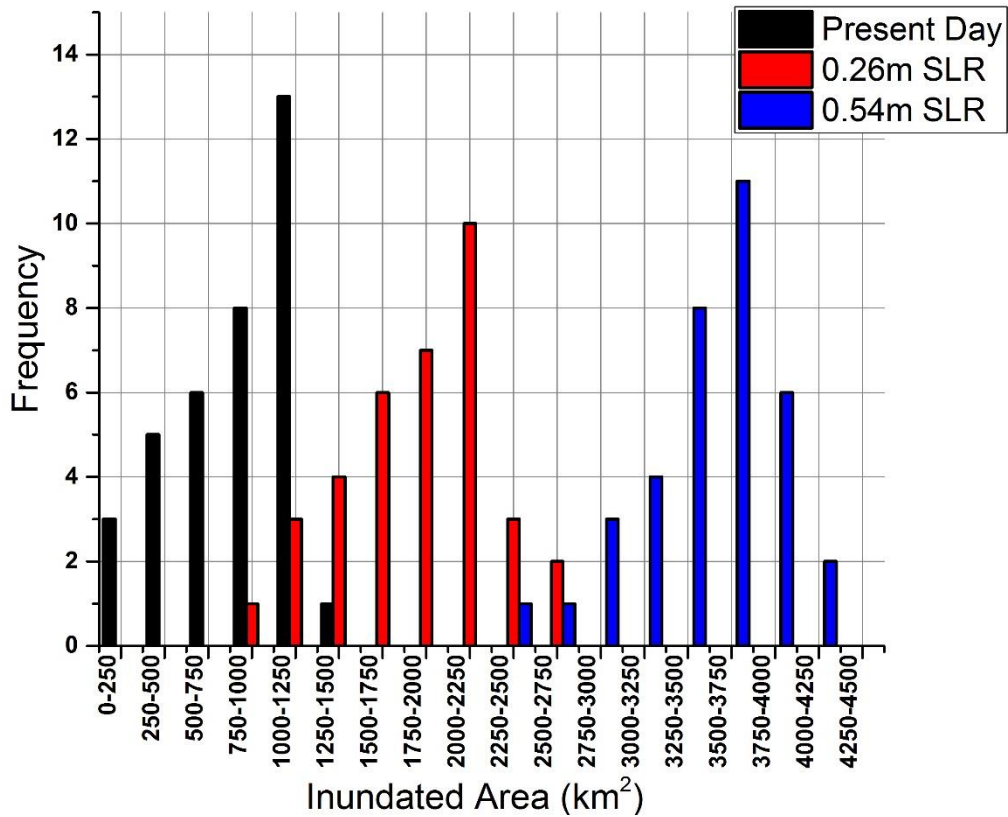


Figure 4. Yellow colors denotes the areas flooded by TC Sidr but not in Aila, and the white color representing the area inundated by TC Aila but not in Sidr. Red color is the area flooded by both TC Sidr and TC Aila. Blue color is showing the non-flooded area (either land or constant water).



501 **Figure 5:** Comparison of inundated area between present-day and future climate scenarios for (a) TC Sidr mid-21st-century
 502 0.26m SLR (b) TC Sidr end-21st-century 0.54m SLR (c) TC Aila mid-21st-century 0.26m SLR (d) TC Aila end-21st-century
 503 0.54m SLR. White color is representing the increased flooded areas that were not in present-day scenario but the increase due
 504 to future SLR. Red color is showing the inundated areas that were similar both for present-day and future SLR scenario case.
 505
 506



507

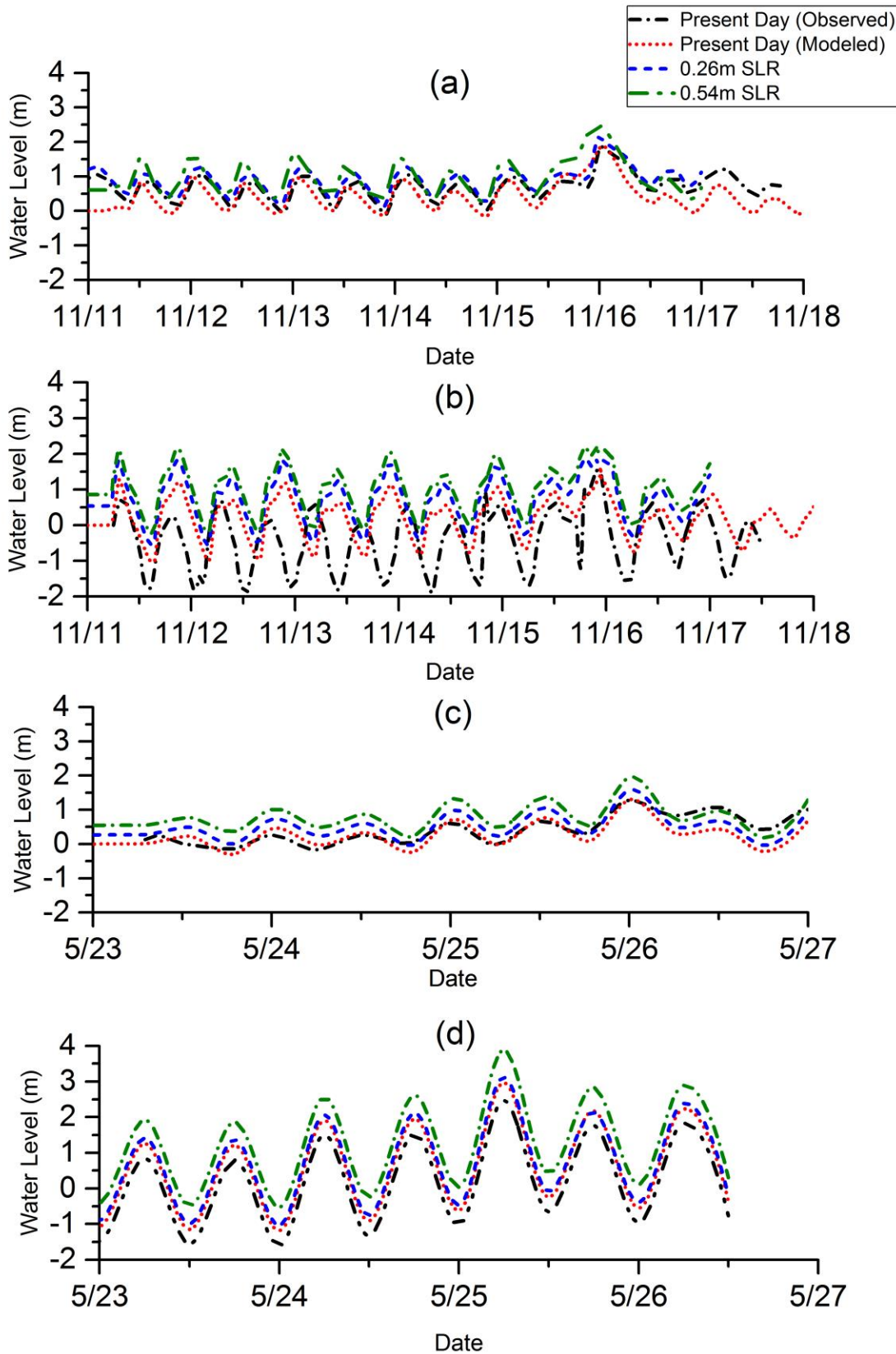
508 **Figure 6:** Ensemble projection of the future SLR impact on storm surge inundation. The column in black color is representing the inundation
 509 events for present-day sea level condition, red colored one is for 0.26 m of SLR and blue colored column is for 0.54 m of SLR conditions. In
 510 total 108 simulations were conducted for present and two future SLR scenarios.

511

512

513

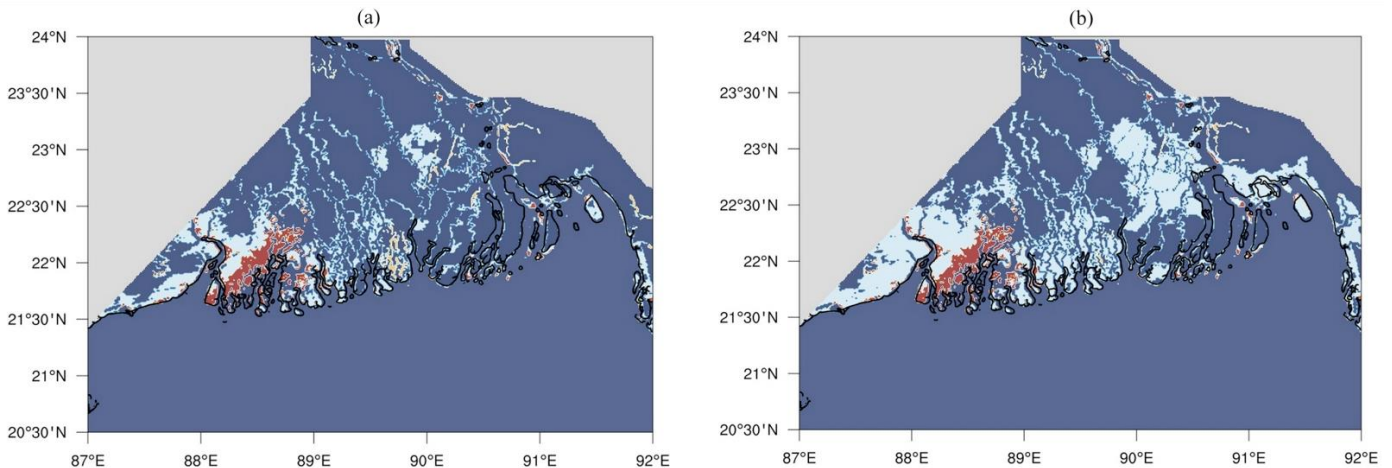
514



515

516 **Figure 7.** Comparison of storm surge water levels between present-day and future SLR scenarios. (a) TC Sidr at Barisal (b) TC Sidr at Charchanga
 517 (c) TC Aila at Barisal (d) TC Aila at Charchanga. The observed, modeled present-day, mid-21st-century and end-21st-century storm surge levels
 518 are denoted by the black dash-dotted, red dotted, blue dashed, and green dash-dotted lines, respectively.

519



521

522 **Figure 8.** Comparison of inundated areas for TC Aila between present-day and end-21st-century (0.54m SLR) scenario. White color is
 523 representing the increased flooded areas that were not in present-day scenario but the increase due to future SLR. Red color is showing the
 524 inundated area that's similar both for present-day and future scenario case. Blue areas are either land or constant waters (those which are already
 525 water at the model initialization time). Figure (a) is representing the inundated area when SLR was considered on ocean depths instead of adding
 526 it in to the open ocean boundary and Figure (b) is showing the inundated area when we considered the SLR on ocean boundary.

527

528

Table 1 Manning's Roughness Coefficient for different land coverings.

| Land cover | Manning's coefficient |
|-----------------|-----------------------|
| River | 0.015 |
| Mangrove | 0.080 |
| Ocean | 0.01 |
| Land | 0.025 |

529

530

Table 2 List of 12 historical TC events used for ensemble projection of storm surge inundation

| Name | Date | Landfall location | Maximum sustained wind (km/h) |
|--------------------------|-------------------------|-------------------|-------------------------------|
| Tropical storm 13 | 14-18 November, 1973 | Noakhali | 102 |
| Cyclone 12 | 23-28 November, 1974 | Bhola | 139 |
| Tropical storm 19 | 07-12 November, 1975 | Chittagong | 93 |
| Tropical storm 1 | 22-25 May, 1985 | Noakhali | 110 |
| Cyclone 4 | 21-30 November, 1988 | Khulna | 205 |
| Cyclone 2 | 22-30 April, 1991 | Chittagong | 235 |
| Cyclone 2 | 26 April – 02 May, 1994 | Cox's Bazar | 215 |
| Cyclone 4 | 18-25 November, 1995 | Cox's Bazar | 190 |
| Cyclone 1 | 13-20 May, 1997 | Noakhali | 165 |

| | | | | |
|-----|-------------------------------|---------------------|------------|-----|
| 531 | Tropical storm 4 | 24-27 October, 2008 | Barguna | 85 |
| 532 | Tropical storm Mahasen | 10-16 May, 2013 | Patuakhali | 85 |
| 533 | Tropical storm Roanu | 18-21 May, 2016 | Chittagong | 110 |

534

535 **Table 3:** Parameters considered for ensemble projection of storm surge inundation which includes the TC intensities, tidal conditions and the
536 SLR scenarios.

| TC name | Intensities | Tide conditions | SLR |
|-------------------------|-------------------------|-------------------------|-----------------------------|
| TC Sidr | +10%, present day, -10% | high, low, actual, zero | present day, 0.26 m, 0.54 m |
| TC Aila | +10%, Present day, -10% | high, low, actual, zero | present day, 0.26 m, 0.54 m |
| 12 historical TC tracks | actual intensities | actual | present day, 0.26 m, 0.54 m |

537

538

539 **Table 4.** Computed values of RMSE, MAE and Nash-Sutcliffe coefficient for both TC Sidr and TC Aila

| Stations | TC Sidr | | | TC Aila | | |
|------------|----------|---------|------|----------|---------|------|
| | RMSE (m) | MAE (m) | NASH | RMSE (m) | MAE (m) | NASH |
| Barisal | 0.23 | 0.16 | 0.85 | 0.33 | 0.24 | 0.65 |
| Charchanga | 0.26 | 0.19 | 0.80 | 0.28 | 0.17 | 0.73 |

Table 5. Comparison of inundated area between present-day & future SLR scenarios and calculated change in percentage with respect to present-day scenario.

| SLR Scenario | TC Sidr | | TC Aila | |
|------------------------------|-----------------------------------|--------------|-----------------------------------|--------------|
| | Inundated Area (km ²) | (%) increase | Inundated Area (km ²) | (%) increase |
| present-day | 1860 | n/a | 1208 | n/a |
| mid-21 st century | 2437 | 31% | 1550 | 28% |
| end-21 st century | 2846 | 53% | 1770 | 47% |

Table 6. Comparison of storm surge level between present day and future SLR scenarios and increase in storm surge level with respect to the present day and SLR scenario for the case of TC Sidr and TC Aila in Barisal and Charchanga observational stations. The SLR scenarios of 0.33 m, 0.40 m and 0.47 m were used to examine the linearity/non-linearity of increase in storm surge level with respect to SLR conditions. In the table "w.r.t" stands for "with respect to".

| SLR (m) | TC Sidr | | | | | | TC Aila | | | | | |
|-------------|----------|--|-------------------------------|------------|---|-------------------------------|--------------|---|-------------------------------|--------------|--|-------------------------------|
| | Barisal | | | Charchanga | | | Barisal | | | Charchanga | | |
| | surge(m) | increase w.r.t present-day (m) and (%) | increase w.r.t. SLR (%) | surge(m) | increase w.r.t. present day (m) and (%) | increase w.r.t. SLR (%) | surge (m) | increase w.r.t. present day (m) and (%) | increase w.r.t. SLR (%) | surge (m) | increase w.r.t present day (m) and (%) | increase w.r.t. SLR (%) |
| 0.00 | 1.87 | n/a | n/a | 1.64 | n/a | n/a | 1.29 | n/a | n/a | 2.50 | n/a | n/a |
| 0.26 | 2.13 | 0.26 (14%) | 100% | 1.87 | 0.23 (14%) | 88% | 1.58 | 0.29 (22%) | 112% | 3.07 | 0.57 (23%) | 219% |
| 0.33 | 2.21 | 0.34 (18%) | 103% | 1.95 | 0.31 (19%) | 94% | 1.66 | 0.37 (29%) | 112% | 3.22 | 0.72 (29%) | 218% |
| 0.40 | 2.26 | 0.39 (21%) | 97% | 2.00 | 0.36 (22%) | 90% | 1.75 | 0.46 (36%) | 115% | 3.42 | 0.92 (37%) | 230% |
| 0.47 | 2.32 | 0.45 (24%) | 96% | 2.08 | 0.44 (27%) | 94% | 1.82 | 0.53 (41%) | 113% | 3.67 | 1.17 (47%) | 249% |
| 0.54 | 2.41 | 0.54 (29%) | 100% | 2.19 | 0.55 (34%) | 102% | 1.96 | 0.67 (52%) | 124% | 3.87 | 1.37 (55%) | 254% |